Type II radio bursts and energetic solar eruptions

N. Gopalswamy,[1] E. Aguilar-Rodriguez,[1,2,3] S. Yashiro,[1,2] S. Nunes,[1,2] M. L. Kaiser,[1] and R. A. Howard[4]

Received 30 March 2005; revised 16 May 2005; accepted 20 May 2005; published 14 October 2005.

[1] We report on a study of type II radio bursts from the Wind/WAVES experiment in conjunction with white-light coronal mass ejections (CME) from the Solar and Heliospheric Observatory (SOHO). The type II bursts considered here have emission components in all the spectral domains: metric, decameter-hectometric (DH) and kilometric (km), so we refer to them as m-to-km type II bursts. CMEs associated with the m-to-km type II bursts were more energetic than those associated with bursts in any single wavelength regime. CMEs associated with type II bursts confined to the metric domain were more energetic (wider and faster) than the general population of CMEs but less energetic than CMEs associated with DH type II bursts. Thus the CME kinetic energy seems to organize the life time of the type II bursts. Contrary to previous results, the starting frequency of metric type II bursts with interplanetary counterparts seems to be no different from that of type II bursts without interplanetary counterparts. We also verified this by showing that the average CME height at the onset time of the type II bursts is the same for the two metric populations. The majority (78%) of the m-to-km type II bursts were associated with solar energetic particle (SEP) events. The solar sources of the small fraction of m-to-km type II bursts without SEP association were poorly connected to the observer near Earth. Finally, we found that the m-to-km type II bursts were associated with bigger flares compared to the purely metric type II bursts.

Citation: Gopalswamy, N., E. Aguilar-Rodriguez, S. Yashiro, S. Nunes, M. L. Kaiser, and R. A. Howard (2005), Type II radio bursts and energetic solar eruptions, *J. Geophys. Res.*, *110*, A12S07, doi:10.1029/2005JA011158.

1. Introduction

[2] Solar radio bursts of type II are indicative of shock propagation in the corona and inner heliosphere, accompanied by electron acceleration [*Wild and McCready*, 1950; *Malitson et al.*, 1973]. Large solar energetic particle (SEP) events are also associated with shocks driven by coronal mass ejections (CMEs), so type II bursts may also indicate shocks that accelerate ions [*Gopalswamy*, 2003; *Gopalswamy et al.*, 2003; *Cliver et al.*, 2004]. Another potential use of type II bursts is that they are good indicators of shocks that eventually cause sudden commencement of geomagnetic storms. Type II radio bursts are electromagnetic in nature, so they arrive at an observer at Earth's orbit in ~8.3 min, providing an advanced warning of the arrival of interplanetary shocks. Traditionally, type II bursts were observed using ground-based radio telescopes, in the frequency range of 150 to 15 MHz: the upper limit is due to the general starting frequency of type II bursts, while the lower limit is due to the ionospheric cutoff because cosmic noise with frequencies below this cutoff cannot penetrate the ionosphere to reach the ground-based instrumentation. The corresponding wavelength range is referred to as the metric (m) domain [*Payne-Scott et al.*, 1947; *Wild and McCready*, 1950]. Type II bursts were also observed at frequencies below the ionospheric cutoff when spaceborne observations became available from IMP-6 [*Malitson et al.*, 1973], Voyager [*Boischot et al.*, 1980], Prognoz [*Pinter et al.*, 1984], ISEE-3 [*Cane and Stone*, 1984], Ulysses [*Hoang and Zlobec*, 1997], and Wind [*Kaiser et al.*, 1998].

[3] Type II radio emission occurs at the local plasma frequency and/or its harmonic, so the frequency of emission is indicative of the heliocentric distance at which the radio emission originates. From the typical density profiles in the corona, one can infer that metric type II bursts are limited to heliocentric distances ~2.5 R_S. Early space observations were obtained at frequencies below 2 MHz, which correspond to radio bursts occurring at heliocentric distances beyond ~10 R_S. The wavelength of type II bursts originating in the heliocentric distance range of 2–10 R_S is in the decameter-hectometric (DH) domain. Information on type II bursts at DH wavelengths became available in quantity for the first time when the Radio and Plasma Wave (WAVES) experiment on board Wind [*Bougeret et al.*, 1995] was launched in 1994. Wind/WAVES operates at frequencies

[1]Laboratory for Extraterrestrial Physics, NASA Goddard Space Flight Center, Greenbelt, Maryland, USA.
[2]Also at Catholic University of America, Washington, D.C., USA.
[3]Also at Intituto de Geofisica, Universidad Nacional Autónomo de México, Mexico City, Mexico.
[4]Naval Research Laboratory, Washington, D.C., USA.

0148-0227/05/2005JA011158$09.00

between 20 kHz and 14 MHz, thus providing information on both DH and kilometric (km) type II bursts [*Reiner et al.*, 1998; *Kaiser et al.*, 1998; *Gopalswamy*, 2004a].

[4] In one of the first studies involving radio data from Wind/WAVES, *Gopalswamy et al.* [1998] noted that none of the 34 metric type II bursts originating from the solar disk had DH counterparts. On the other hand, there were interplanetary (IP) shocks detected in situ, apparently not associated with the metric type II bursts but occurring within the same study period. Their analysis also indicated that the IP shocks and metric type II bursts in their data set did not come from the same solar source. *Gopalswamy et al.* [2001a] repeated their study of metric type II bursts and their association with IP events. They found that 93% of metric type II bursts did not have in situ IP events (shocks or ejecta) and a similar fraction (80%) of IP events had no metric counterparts. Association of metric type II bursts with DH (18%) and kilometric (25%) type II bursts was also rather poor. Only a small fraction (9%) of metric type II bursts originating from the disk (central meridian distance, CMD $<60^\circ$) were associated with IP shocks; in each of these cases, a halo or partial halo CME was involved (width $>120^\circ$) and an IP type II burst was present. A CME that appears to surround the occulting disk is known as a halo [*Howard et al.*, 1982].

[5] Halo and partial halo CMEs observed by SOHO during cycle 23 are faster and wider than the average CME [*Yashiro et al.*, 2004; *Gopalswamy*, 2004b]. The CMEs associated with DH type II bursts are also faster and wider on the average [*Gopalswamy et al.*, 2001b]. Wider CMEs are generally more massive, so fast and wide CMEs are more energetic than the general population. On the other hand, CMEs associated with DH type II bursts are more energetic than the metric type II-associated CMEs [*Lara et al.*, 2003]. Thus there seems to be a hierarchical relationship among type II bursts in various wavelength domains, organized by the CME kinetic energy. The connection between CME energy and the type II wavelength domain can be understood as follows: The wavelength domain reflects the heliocentric distance at which the underlying shock is located, so the higher the kinetic energy of the CME, the larger the heliocentric distance the shock can reach. In this paper we verify this possibility using a large number of type II events with counterparts in all three wavelength domains.

2. Data Selection

[6] We are interested in the hierarchical relationship between type II bursts in terms of properties of the associated CMEs. For this purpose, we consider three populations of CMEs associated with type II bursts: (1) in the metric domain with no counterparts in the DH and km domains; (2) in DH domain irrespective of counterparts in the m and km domains; (3) with counterparts in all of the wavelength domains, from metric to DH to km. We refer to the population 3 as m-to-km type II bursts. The three populations will also be compared with the general population of ~9000 CMEs observed by SOHO up to the end of 2004. We restrict the list of metric type II bursts to limb events (solar source, as identified from H-alpha flare locations, must be within 30° from the limb) for an unambiguous identification of CMEs. The visibility of CMEs associated with metric type II bursts originating from close to the disk center may be limited by the presence of the coronagraph occulting disk [*Cliver et al.*, 1999; *Gopalswamy et al.*, 2001a]. The study period is from 1996 to the end of 2004. We excluded type II bursts during the two major SOHO data gaps in June–October 1998 and January 1999.

[7] The list of metric type II bursts was obtained from the Solar Geophysical Data (SGD) and from the individual observatory Web sites. The list of DH type II bursts was obtained from the online catalog from Wind/WAVES (available at http://lep694.gsfc.nasa.gov/waves/waves.html) with the criterion that the burst must have been observed in the 1–14 MHz range. The list of m-to-km type II bursts was obtained by combining the two data sources and choosing only those events that have type II signatures in the metric, DH, and kilometric domains. The DH and km type II bursts were observed by the RAD2 (1.075–13.825 MHz) and RAD1 (20–1040 kHz) receivers of the WAVES experiment. The RAD2 spectral range corresponds to 21.7 to 279 m (decameter-hectometric or DH wavelength range). The spectral range of the RAD1 receiver starts in the hectometric range (288.5 m) and ends in the km domain (15 km). Thus our selection criterion requires that there should be type II signatures detected by ground based instruments as well as by both receivers of the WAVES experiment. When there is data overlap between radio and white light observations, every type II burst in the DH domain is known to be associated with a white-light CME [*Gopalswamy et al.*, 2000; *Reiner*, 2000; *Gopalswamy et al.*, 2001b]. CMEs are thought to drive shocks, which accelerate electrons that result in the observed type II radio emission via plasma emission processes. For this study we use CME data obtained by the Solar and Heliospheric Observatory (SOHO) mission's Large Angle and Spectrometric Coronagraph (LASCO) [*Brueckner et al.*, 1995]. CMEs propagating from about 2 to 32 R_S from the Sun center are imaged by LASCO, providing basic attributes such as speed, acceleration, width, and apparent latitude of CMEs. The LASCO field of view overlaps with the spatial domain in which the WAVES type II radio emission originates, establishing the study of the connection between CMEs and radio bursts.

[8] In all, we identified 132 metric type II bursts that originated from close to the solar limb. We refer to these bursts as m-limb events. All the m-limb type II bursts were associated with LASCO CMEs when there was data overlap. Over the same period, there were 221 DH type II bursts overlapping with SOHO data. For each one of type II bursts, a CME was uniquely identified. The m-to-km type II bursts were smallest in number (71) and are listed in Table 1, with the date in column 2. The starting times and frequencies (Fs in MHz) of the metric type II bursts are given in column 3 and 4, respectively. The listed Fs correspond to the fundamental emission (plasma frequency ~ observing frequency). Fs suffixed with a question mark means we do not know whether the burst is in the fundamental or harmonic mode. The subsequent type II activity in the DH and km wavelengths is shown by the start time (column 5) and frequency range (column 6).

Table 1. List of m-to-km Type II Bursts With the Properties of the Associated Flares and CMEs

		Type II (metric)		Type II (DH-km)		Flare				CME							
	Date	Time	Fs	Time	F range	Time	Imp	Loc.	AR#	Time	CPA	W	V	a	HT1	HT2	SEP
01	1997/05/12	04:54	90	05:15	12-0.08	04:42	C1.3/?	N21W08	8038	05:30	360	360	464	−15.0	2.6	1.0	2
02	1997/05/21	20:10	70	20:20	5-0.5	20:03	M1.3/SF	N05W12	8040	21:00	269	60	296	1.4	1.3	1.8	N
03	1997/11/03	04:37	130	05:15	14-0.25	04:32	C8.6/SB	S18W16	8100	05:28	240	109	227	1.4	2.6	2.8	N
04	1997/11/04	05:58	115	06:00	14-0.10	05:52	X2.1/2B	S14W34	8100	06:10	360	360	785	−22.1	3.1	2.1	72
05	1997/11/06	11:53	245?	12:20	14-0.10	11:49	X9.4/2B	S18W63	8100	12:10	360	360	1556	−44.1	3.1	2.5	490
06	1998/04/20	09:56	60?	10:25	10-0.03	09:38	M1.4/?	S44W90	8194	10:07	284	165	1863	43.5	1.0	1.5	1700
07	1998/04/23	05:40	45	06:00	14-0.02	05:35	X1.2/?	S17E91	8210	05:27	360	360	1618	18.5	3.5	3.6	HiB
08	1998/05/09	03:26	75	03:35	9-0.40	03:04	M7.7/?	S15W86	8210	03:35	262	178	2331	−140.5	1.1	0.2	12
09	1998/06/16	18:18	90?	18:20	12-0.05	18:03	M1.0/?	S17W90	8232	18:27	341	281	1484	−74.7	3.5	2.4	2
10	1999/05/03	05:43	90	05:50	8-0.20	05:36	M4.4/2N	N15E32	8525	06:06	360	360	1584	15.8	−0.1	0.2	14
11	1999/05/27	10:46	60?	10:55	14-0.07	—	—	W-limb	—	11:06	360	360	1691	−33.5	1.9	1.5	9
12	1999/06/04	07:02	90	07:05	14-0.06	06:52	M3.9/2B	N17W69	8552	07:26	289	150	2230	−158.8	4.5	2.8	64
13	1999/06/11	11:15	85	11:45	14-0.40	11:07	C8.8/?	N38E90	8585	11:26	35	181	1569	−20.8	1.3	1.0	N
14	2000/01/18	17:19	80?	17:31	14-0.50	17:07	M3.9/1N	S19E11	8831	17:54	360	360	739	−7.1	1.8	1.4	1
15	2000/02/08	08:52	123	09:05	12-0.02	08:42	M1.3/1B	N25E26	8858	09:30	360	360	1079	−35.3	0.1	−1.2	N
16	2000/02/12	04:03	90	03:55	4-0.40[a]	03:51	M1.7/1N	N25W23	8858	04:31	360	360	1107	−8.3	0.8	0.4	2
17	2000/02/17	20:25	90	20:42	14-0.10	20:17	M1.3/2N	S29E07	8872	21:30	360	360	728	−22.9	2.1	0.5	1
18	2000/05/07	20:45	300?	21:15	14-0.50	—	—	W-limb	8970?	20:50	360	360	1781	−71.8	2.9	2.2	N
19	2000/06/06	15:16	146?	15:20	14-0.00	14:58	X2.3/3B	N33E25	9026	15:54	360	360	1119	1.5	0.4	0.5	84
20	2000/07/14	10:18	175	10:30	14-0.08	10:03	X5.7/3B	N22W07	9077	10:54	360	360	1674	−96.1	0.0	−0.8	24000
21	2000/09/12	11:33	90	12:00	14-0.06	11:31	M1.0/2N	S17W09	DSF	11:54	360	360	1550	58.2	−0.7	0.4	320
22	2000/09/16	04:11	90	04:30	14-0.40	04:06	M5.9/2B	N14W07	9165	05:18	360	360	1215	−12.3	2.1	1.5	HiB
23	2000/11/24	05:02	90	05:10	14-0.10	04:55	X2.0/3B	N19W06	9236	05:30	360	360	994	72.0	0.5	3.8	8
24	2000/11/24	15:07	180?	15:25	14-0.20	14:51	X2.3/2B	N22W07	9236	15:30	360	360	1245	−3.3	0.8	0.7	94
25	2001/01/20	21:12	160	21:30	14-0.50	21:06	M7.7/2B	S07E46	9313	21:30	360	360	1507	−41.1	1.5	0.7	2
26	2001/01/26	11:55	60	12:06	14-0.40	11:50	C1.6/SF	S23W57	9320	12:06	276	176	928	−15.3	2.5	1.8	N
27	2001/03/29	10:03	175	10:12	4-0.06	09:57	X1.7/SF	N20W19	9402	10:26	360	360	942	3.5	1.8	2.0	35
28	2001/04/02	21:49	140	22:05	14-0.25	21:32	X20/?	N19W72	9393	22:06	261	244	2505	108.5	2.2	2.9	1100
29	2001/04/09	15:25	133	15:53	12-0.10	15:20	M7.9/2B	S21W04	9415	15:54	360	360	1192	1.3	0.3	0.3	5
30	2001/04/10	05:13	90	05:24	14-0.10	05:06	X2.3/3B	S23W09	9415	05:30	360	360	2411	211.6	−0.8	0.3	355
31	2001/04/15	13:47	180?	14:05	14-0.04	13:19	X14.4/2B	S20W85	9415	14:06	245	167	1199	−35.9	2.5	2.0	951
32	2001/04/18	02:17	130	02:55	1-0.10	01:33	B9.1/?[b]	S23W120	9424	02:30	360	360	2465	−9.5	2.2	2.2	321
33	2001/08/25	16:32	180?	16:50	8-0.17	16:23	X5.3/3B	S17E34	9591	16:50	360	360	1433	−46.8	2.1	1.3	HiB
34	2001/10/09	10:52	85	11:15	8-0.20	10:46	M1.4/2F	S28E08	9653	11:30	360	360	973	−41.5	1.9	0.2	5
35	2001/10/19	16:24	180?	16:45	14-0.03	16:13	X1.6/2B	N15W29	9661	16:50	360	360	901	−0.7	1.2	1.2	11
36	2001/10/25	14:55	180?	15:30	14-0.03	14:42	X1.3/2B	S16W21	9672	15:26	360	360	1092	−1.4	0.4	0.3	HiB
37	2001/11/04	16:10	180?	16:30	14-0.07	16:03	X1.0/3B	N06W18	9684	16:35	360	360	1810	−63.4	0.7	−0.3	31700
38	2001/11/22	22:31	116	22:40	14-0.04	22:32	M9.9/?	S17W38	9704	23:30	360	360	1437	−12.9	−2.2	−2.8	18900
39	2001/12/11	08:03	135	12:45	4.5-0.8[a]	07:58	X2.8/SF	N16E41	9733	08:30	23	142	804	−9.6	1.1	0.9	1
40	2001/12/26	05:12	90	05:20	14-0.15	04:32	M7.1/1B	N08W54	9742	05:30	281	212	1446	−39.9	1.7	1.3	779
41	2001/12/28	19:59	65?	20:35	14-0.35	20:02	X3.4/?	S26E90	9756	20:30	360	360	2216	6.9	−0.5	−0.4	76
42	2002/01/14	06:08	90	06:25	12-0.10	05:29	M4.4/?	S28W83	9772	05:35	360	360	1492	52.3	5.5	5.4	HiB
43	2002/03/22	11:08	70	11:30	14-0.50	10:12	M1.6/?	S09W90	9866	11:06	360	360	1750	−22.5	3.4	3.4	16
44	2002/04/17	08:08	40	08:30	5-0.04	07:46	M2.6/2N	S14W34	9906	08:26	360	360	1240	−19.8	1.9	1.3	24
45	2002/04/21	01:18	90	01:30	10-0.06	00:43	X1.5/1F	S14W84	9906	01:27	360	360	2393	−1.4	1.3	1.3	2520
46	2002/07/23	00:28	170	00:50	11-0.40	00:18	X4.8/2B	S13E72	0039	00:42	360	360	2285	—	1.2	−1.0	HiB
47	2002/08/16	05:52	95	06:15	14-0.30	05:46	M2.4/SF	N07W83	0061	06:06	293	162	1378	−3.7	0.8	0.7	N
48	2002/08/16	12:06	180	12:20	14-0.06	11:32	M5.2/2N	S14E20	0069	12:30	360	360	1585	−67.1	0.6	−0.6	4
49	2002/08/24	01:01	120	01:45	5-0.40	00:49	X3.1/1F	S02W81	0069	01:27	360	360	1913	43.7	1.5	2.1	317
50	2002/09/05	16:33	250?	16:55	16-0.03	16:18	C5.2/SF	N09E28	0102	16:54	360	360	1748	43.0	1.0	1.4	208
51	2002/10/27	22:58	100	23:06	14-0.30	—	C3.0/-?	N16E74	—	23:18	360	360	2115	75.1	3.6	4.1	N
52	2002/11/09	13:17	85?	13:20	14-0.10	13:08	M4.6/2B	S12W29	0180	13:31	360	360	1838	35.4	1.7	2.1	404
53	2002/11/10	03:14	90	03:20	3-0.30	03:04	M2.4/2N	S12W37	0180	03:30	360	360	1670	−54.6	2.7	2.2	HiB
54	2003/03/18	12:16	80?	12:25	4.5-0.5	11:51	X1.5/1B	S15W46	0314	12:30	263	209	1601	−13.3	1.6	1.4	N
55	2003/04/22	07:16	70	07:25	3.5-0.7	—	—	E-limb	—	07:36	87	171	918	−8.9	1.7	1.3	N
56	2003/05/28	00:26	180?	01:00	1-0.20	00:17	X3.6/?	S06W21	0365	00:50	360	360	1366	25.9	1.5	2.3	121
57	2003/05/29	01:06	90	01:10	13-0.20	00:51	X1.2/2B	S06W37	0365	01:27	360	360	1237	−22.3	3.1	2.6	HiB
58	2003/05/31	02:23	180	03:00	1-0.15	02:13	M9.3/2B	S07W65	0365	02:30	360	360	1835	−2.4	1.4	1.4	27
59	2003/06/15	23:46	180?	00:00	14-0.4	23:25	X1.3/SF	S07E80	0386	23:54	360	360	2053	−0.9	2.1	2.1	N
60	2003/06/17	22:48	180	22:50	10-0.20	22:27	M6.8/?	S08E59	0386	23:18	360	360	1813	−2.9	2.4	2.4	24
61	2003/10/28	11:02	180?	11:10	14-40	09:51	X17.2/4B	S16E08	0486	11:30	360	360	2459	−105.2	0.1	−0.8	29500
62	2003/10/29	20:40	80?	20:55	11-0.50	20:37	X10.0/2B	S15W02	0486	20:54	360	360	2029	−146.5	0.8	−0.1	HiB
63	2003/11/02	17:14	180	17:30	12-0.25	17:03	X8.3/2B	S14W56	0486	17:30	360	360	2598	−32.4	−0.3	−0.4	HiB
64	2003/11/03	09:50	225	10:00	6-0.40	09:43	X3.9/2F	N08W77	0488	10:06	293	103	1420	−11.6	0.6	0.4	HiB

Table 1. (continued)

		Type II (metric)		Type II (DH-km)		Flare				CME							
	Date	Time	Fs	Time	F range	Time	Imp	Loc.	AR#	Time	CPA	W	V	a	HT1	HT2	SEP
65	2003/11/04	19:42	180?	20:00	10-0.20	19:29	X28.0/3B	S19W83	0486	19:54	360	360	2657	434.8	0.8	1.9	353
66	2004/01/07	03:58	230	04:15	14-0.75	03:43	M4.5/2N	N02E82	0537	04:06	78	171	1581	−60.4	2.5	1.9	N
67	2004/09/12	00:23	55	00:45	14-0.04	00:04	M4.8/2N	N04E42	0672	00:36	360	360	1328	22.5	0.1	0.5	273
68	2004/11/01	03:21	125	05:55	3-0.40	03:04	M1.1/1F	N15W41	0691	03:54	242	192	459	−6.6	1.9	1.7	63
69	2004/11/06	00:37	40	01:50	6-0.70	00:11	M9.3/2N	N10E08	0696	01:31	37	178	818	−81.5	−0.1	−1.7	N
70	2004/11/07	15:59	180?	16:25	14-0.06	15:42	X2.0/?	N09W17	0696	16:54	360	360	1759	−19.7	−2.5	−3.1	495
71	2004/12/30	22:11	180?	23:45	5-0.70	22:04	M4.2/2N	N04E46	0715	22:30	360	360	1035	−0.6	0.6	0.6	N

[a]The m-km association may be fortuitous due to multiple CMEs from different regions.
[b]The X-ray flare size is underestimate because the source is ~30 degrees behind the limb.

Onset time (columns 7), X-ray/Optical importance (column 8), heliographic location (column 9), and the NOAA active region number (column 10) of the associated flare are also listed. Columns 11–15 give the information of the associated CMEs in the following order: UT, central position angle (CPA), width (W°), speed (V km s^{-1}), and acceleration (a ms^{-2}). The CME height (in solar radii, R_S) at the start time of the metric type II burst is also given (column 16 with linear fit (HT1) and column 17 with quadratic fit (HT2)). The last column (18) gives the intensity of the associated solar energetic particle (SEP) event measured in particle flux units (pfu, protons per (cm^2 s sr) in the >10 MeV GOES channel). Appropriate notation is made when there is no SEP event (N) or when the background is high (HiB).

3. Analysis and Results

3.1. Illustrative Examples

[9] Figure 1 shows an example of a metric type II burst without longer wavelength counterparts. The m type II originated from AR 0123 located at N16E61 on 4 December 2002. The location of the eruption site can be seen in the difference image obtained by the Extreme-ultraviolet Imaging Telescope (EIT) [*Delaboudiniere et al.*, 1995]. The CME was 162° wide and had a linear speed of 825 km/s. Even though the final width was large, it was relatively small early on. The CME was also decelerating with an average value of 13 ms^{-2}. When the metric type II started, the CME leading edge was at a height of 2.7 R_S. Figure 2 shows a type II burst confined to the DH domain, associated with a CME from AR 9481 at the east limb on 30 May 2001. The CME was very fast (2087 km/s), wide (216°), and rapidly decelerating (−45 ms^{-2}). Any associated flare seems to have been occulted. Figure 3 shows the type II burst on 26 December 2001, which has counterparts in all the three wavelength domains. The metric type II burst started at 0512 UT. The associated CME was very fast (1446 km/s) and a partial halo (width 212°) and originated from AR 9742 (N08W54). Extrapolating the CME height-time plot to the time of metric type II onset, we find that the CME leading edge was at a height of 1.6 R_S. The type II burst can be seen to continue into DH and km domains. The times corresponding to the three frames of LASCO images in Figure 3 are marked on the dynamic spectrum showing approximate height in the corona from which the radio emission originates. For example, at the time of the last frame at 0743 UT, the CME was at a height of 20.5 R_S and the type II radio emission occurs at 800 kHz. This means that the CME-driven shock is crossing the corona where the local density is 7.9×10^3 cm^{-3}.

3.2. Hierarchy of Type II Bursts

[10] Figure 4 compares the CME properties of m, DH, and m-to-km type II bursts. We have shown the three basic attributes, namely, speed, width, and acceleration for four populations: (1) all CMEs up to the end of 2004, (2) CMEs associated with metric limb (m-limb) type II bursts, (3) CMEs associated with DH type II bursts, (4) CMEs associated with m-to-km type II bursts. All of the parameters were measured in the sky plane, and no attempt was made to correct for projection effects. The speeds were obtained by fitting a straight line to the height-time measurements and hence represent the average speeds within the LASCO field of view. The average widths shown on the plots were obtained by excluding full halo CMEs (apparent width = 360°) because it is difficult to assess the true width of halo CMEs. The average CME speeds were 487, 610, 1115, and 1490 km/s for the general population, metric-associated, DH-associated, and m-to-km associated CMEs, respectively. The median values had a similar progressive increase. The corresponding average CME widths were 56° (general population), 85° (metric-associated), 139° (DH-associated), and 171° (m-to-km associated), counting only the nonhalo CMEs. The fraction of full halo CMEs also progressively increased; among the metric-associated CMEs, there were 4.7% full halos compared to the 3% for the general population. However, nearly half of the DH-associated CMEs (or 47.5%) had full halos, while 71.2% of CMEs associated with m-to-km type II bursts were full halos. As for acceleration, the average value was negative for all of the distributions, although the median value for the general population was ~0. The average deceleration also progressively increased: from the general population (−2 ms^{-2}) to the metric-associated CMEs (−3 ms^{-2}), to the DH (−7 ms^{-2}) and finally to the m-to-km CMEs (−11 ms^{-2}), the CMEs had larger decelerations. Thus there is a clear trend of progressively increasing average values of speed, width, deceleration, and fraction of full halos as one goes from the general population to the one associated with m-to-km type II bursts. The larger deceleration for faster CMEs is expected because of the aerodynamic drag faced by CMEs as they propagate into the corona and IP medium. Thus one can say that a combination of CME speed and width organizes the three populations of type II bursts.

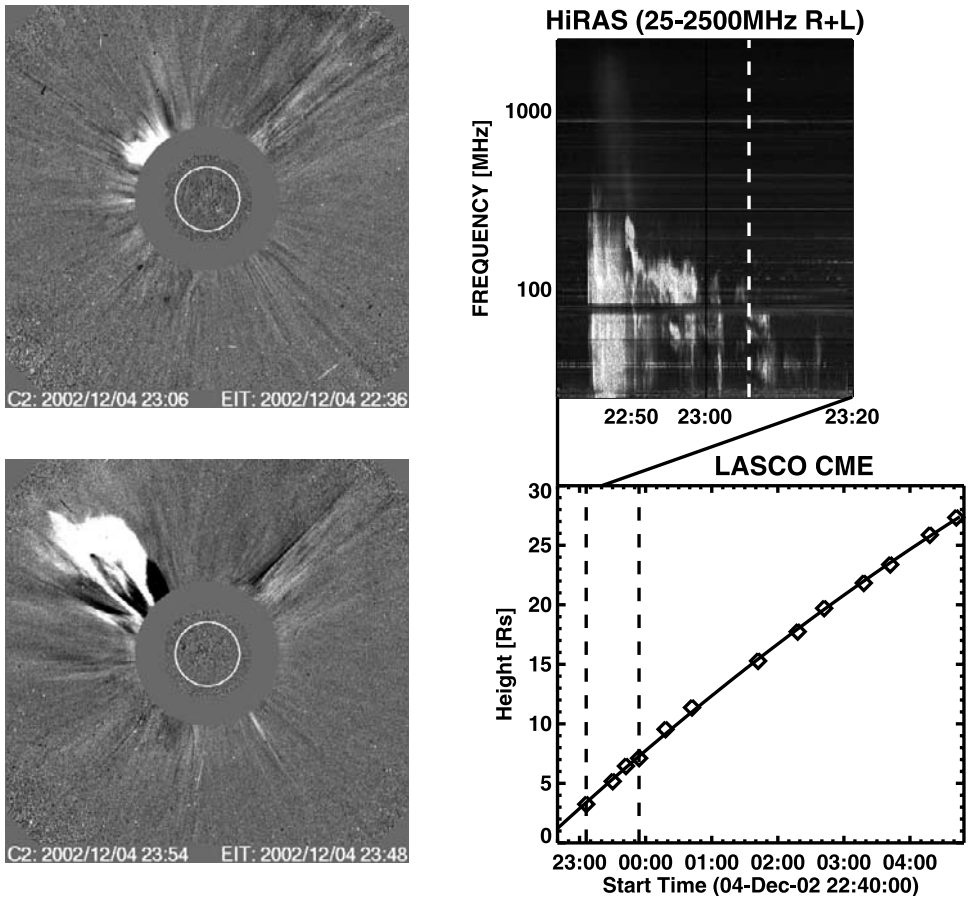

Figure 1. Metric type II burst (upper right panel) on 2002/12/04 obtained by the Hiraiso radio spectrograph (HiRAS) and snapshots of the associated coronal mass ejection (CME) (left panels) at 2306 and 2354 UT. The height-time plot of the CME is shown in the bottom right panel. The time of the first LASCO difference image (2306 UT) is marked on the type II dynamic spectrum by a vertical dashed line. Times of both the LASCO frames are also marked on the height-time plot. The type II was associated with a CME of speed 825 km/s and a width of 162 deg from AR 0123 located at N16E61. At 2306 UT, the CME leading edge was already at a height of 3.25 R_S. When the type II started, the CME leading edge was at a height of 2.7 R_S. See color version of this figure in the HTML.

There is also a clear relationship between CME mass and width: wider CMEs are generally more massive. Therefore faster and wider CMEs can be taken to suggest that these CMEs are more energetic on the average. Thus the CME kinetic energy essentially organizes the three type II populations: metric, DH, and m-to-km. CMEs associated with metric type II bursts with no IP counterparts are more energetic than the general population. On the other hand, CMEs associated with DH type II bursts are more energetic than the ones associated with metric type II bursts but less energetic compared to the m-to-km type II bursts.

3.3. Association With SEP Events

[11] The last column of Table 1 gives the SEP association for the 71 m-to-km type II bursts. There are three types of entries in this column: (1) If there is a clear SEP, event, then the peak intensity of protons in the >10 MeV channel is listed in units of pfu. (2) If the preevent SEP level is higher than the nominal threshold (~0.1 pfu) of the GOES detector, then it is difficult to decide the association, so we indicate that there was high background (HiB). (3) If there is no enhancement above the threshold, we list the event as "N" for no SEP association. The background SEP level was high for 11 events. Of the remaining 60 events, 13 did not have SEP intensity above the GOES instrument threshold (~0.1 pfu). All of the remaining 47 m-to-km type II bursts had SEP association. Thus the majority (47/60 or 78%) of the m-to-km type II bursts were associated with SEP events. This is not surprising because the speed and width distribution of CMEs associated with SEP events [*Gopalswamy et al.*, 2004] and m-to-km type II bursts (see Figure 4) are nearly identical. Figure 5 shows the distributions of speed, width, and acceleration of all the large SEP events up to the end of 2004. There were 72 events in all that had simultaneous SOHO observations. The average speed of SEP-associated CMEs (1446 km/s) is nearly identical to that of CMEs associated with the m-to-km type II bursts (1490 km/s, see Figure 4) over the same period. The fraction of full halos in the SEP events and the mean and median widths are all similar to the corresponding values of the CMEs associated with m-to-km type II bursts. Finally, the average acceleration (-11 m s^{-2}) is also the same for CMEs associated with SEP events and m-to-km type II bursts.

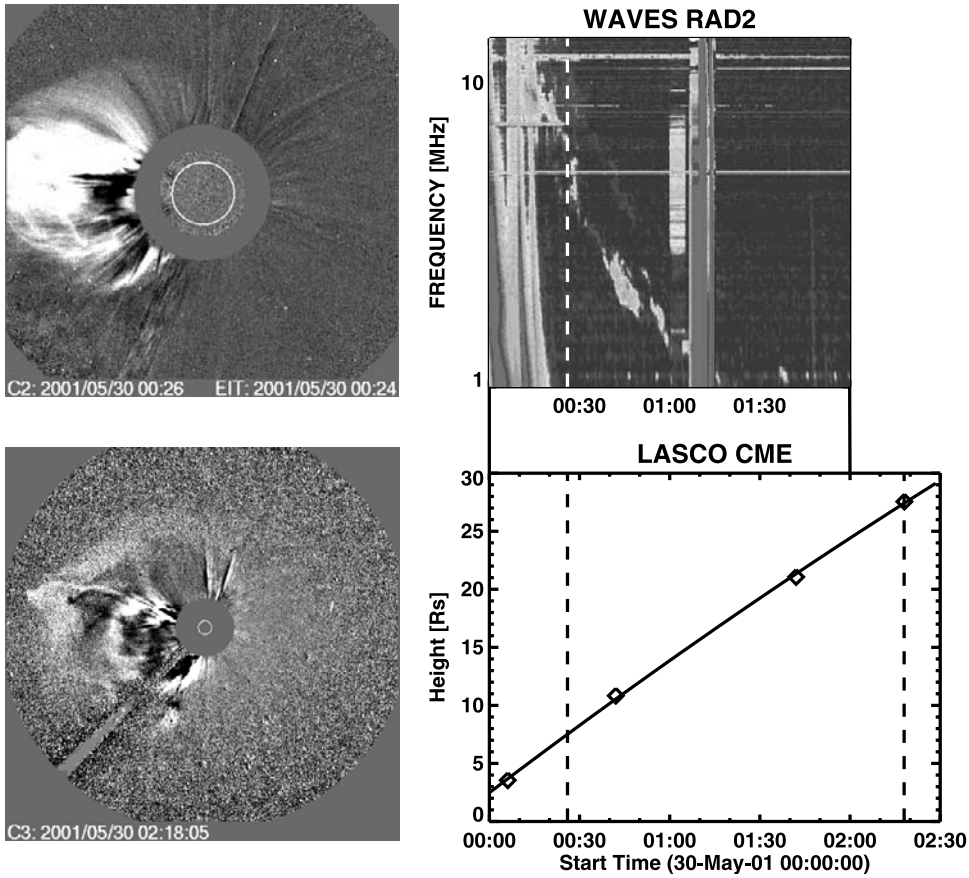

Figure 2. Example of a type II burst confined to the DH domain along with two snapshot mages of the associated CME. The CME clearly originated from slightly behind the east limb as the EIT difference image shows. No metric type II burst was reported for this event, but the type III bursts in the WAVES dynamic spectrum had metric counterparts. One cannot rule out the possibility of weak metric type II burst superposed on the type III bursts. This means the type II burst is clearly observed only in the DH domain. The type II burst had fundamental-harmonic structure below 10 MHz. Above this frequency, the space between the fundamental and harmonic components was filled, which is an indication of CME interaction, which we confirmed from LASCO observations. The leading edge of the CME just crossed the LASCO/C2 field of view at 0026. It was a very fast CME (speed $\sim$ 2087 km/s, width $\sim$ 216°). As in Figure 1, the times of the LASCO frames are marked on the dynamic spectrum. When the type II burst crossed the lower edge of the RAD2 spectral domain at $\sim$0130 UT, the CME was already at a height of 18 R_S. Since the CME originates close to the limb, the measured speed and height are likely to be close to the actual values. Without spatial resolution, it is difficult to say where the type II burst is located with respect to the CME, one can infer that the height of the burst may not exceed 18 R_S. The type II burst was not observed in the RAD1 spectral domain even though the RAD1 receiver is more sensitive. This means the type II burst has weakened to the background level around this time. The LASCO/C3 frame at 0218 UT shows that the leading edge was at a height of 27.6 R_S, close to the edge of the field of view. The shock probably weakened quickly in this event because it was propagating through a tenuous medium. See color version of this figure in the HTML.

[12] Why did the 13 m-to-km type II bursts lack SEP events, even though the associated CMEs were fast and wide? We have shown the distribution of the solar-source longitudes of the m-to-km and SEP CMEs in Figure 6. The two distributions differ in the following aspects: (1) the SEP source longitudes are preferentially in the western hemisphere, with the number of events dropping significantly to the east of W10. Only 13.8% of SEP events originated east of W10. Western source regions are better connected to a near-Earth observer than the eastern ones. The drop is much shallower for the m-to-km events and a larger fraction (33.8%) of them had longitudes east of W10. (2) There are more SEP events from behind the west limb than the m-to-km events. This longitude dependence was also shown recently by *Cliver et al.* [2004] for m-to-DH events.

[13] There is a conspicuous peak near the disk center in the longitudinal distribution of m-to-km burst sources (Figure 6a), which suggests that the radio emission is more easily seen when the CME is Earth-directed. For limb events, the farside shock flank would be hidden (the radiation may not penetrate the CME plasma), so the

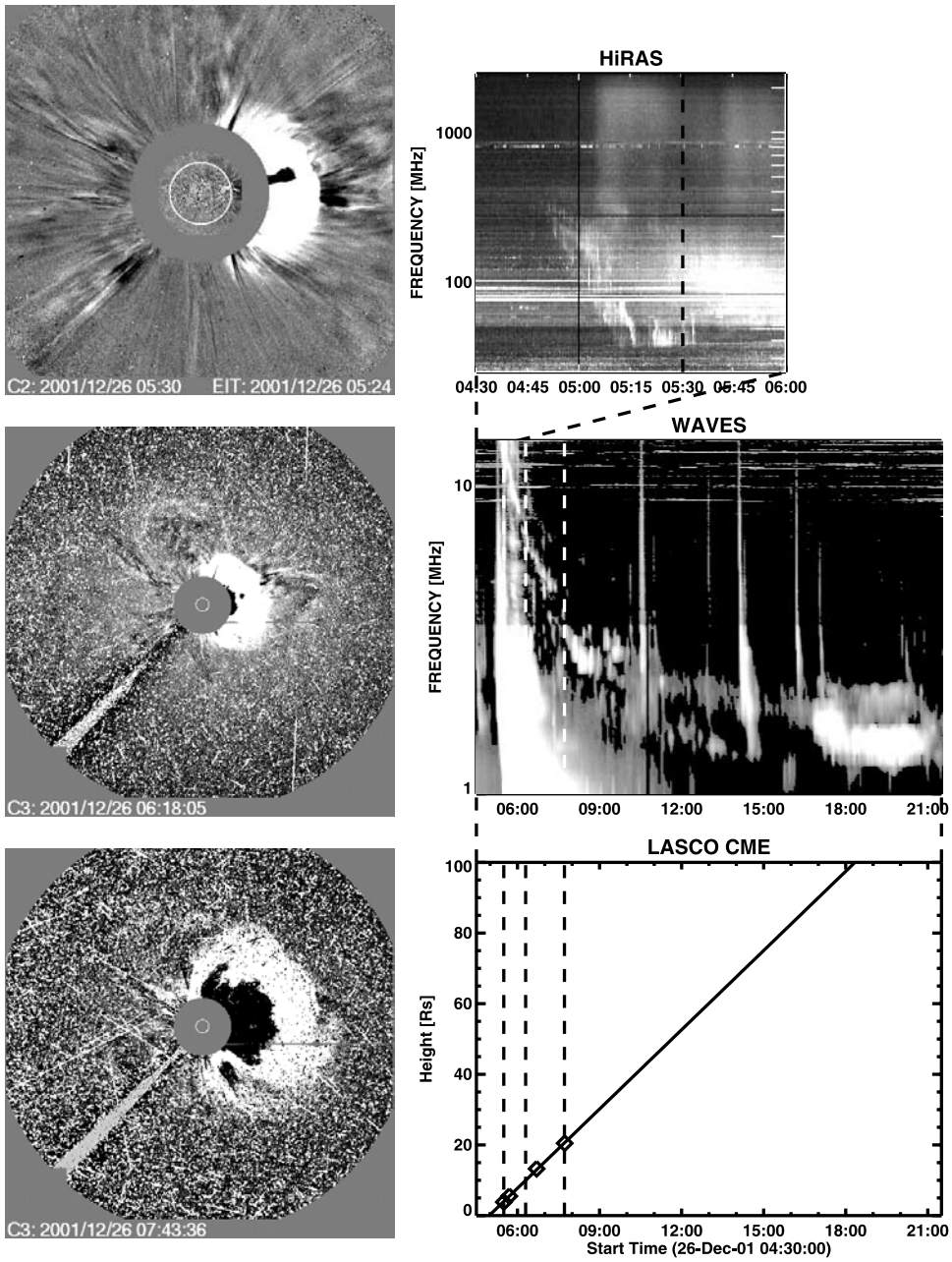

Figure 3. Example of a type II event with counterparts in all the wavelength domains from HiRAS (top right) and WAVES (middle right) observations. Three LASCO frames are shown in the left panels, which were taken when the type II burst was in the metric, DH, and km domains. The times of the LASCO frames are shown by the vertical dashed lines superposed on the dynamic spectra. The CME responsible for the radio burst was a partial halo CME (width $\sim 212°$) from N08W54 (AR 9742) close to the west limb with an average speed of 1446 km/s. The CME was also associated with a large solar energetic particle event, which degraded the image quality in the second and third LASCO frames shown. In fact, it was not possible to measure the CME beyond 20.5 R_S. See color version of this figure in the HTML.

intensity and hence the detectability of these bursts would be reduced.

[14] The difference in the source longitude distributions is likely to be one of the major reasons for the lack of SEP events in some m-to-km events. When we examined the source longitudes of the 13 m-to-km CMEs not associated with SEP events, we found that six of them were eastern events (14, 16, 52, 61, 69, 74). For four western m-to-km CMEs without SEPs, the speeds [296 (02), 227 (03), 928 (27), and 1378 km/s (48)] were well below the average (1481 km/s). Two of the western events without SEPs originated from behind the limb (19, 57) and one of them (57) had below-average speed (918 km/s). The remaining event on 18 March 2003 at 1230 UT (54) was western (S15W46), and the associated CME was relatively fast (1601 km/s) and wide (209°). There was a large gap in

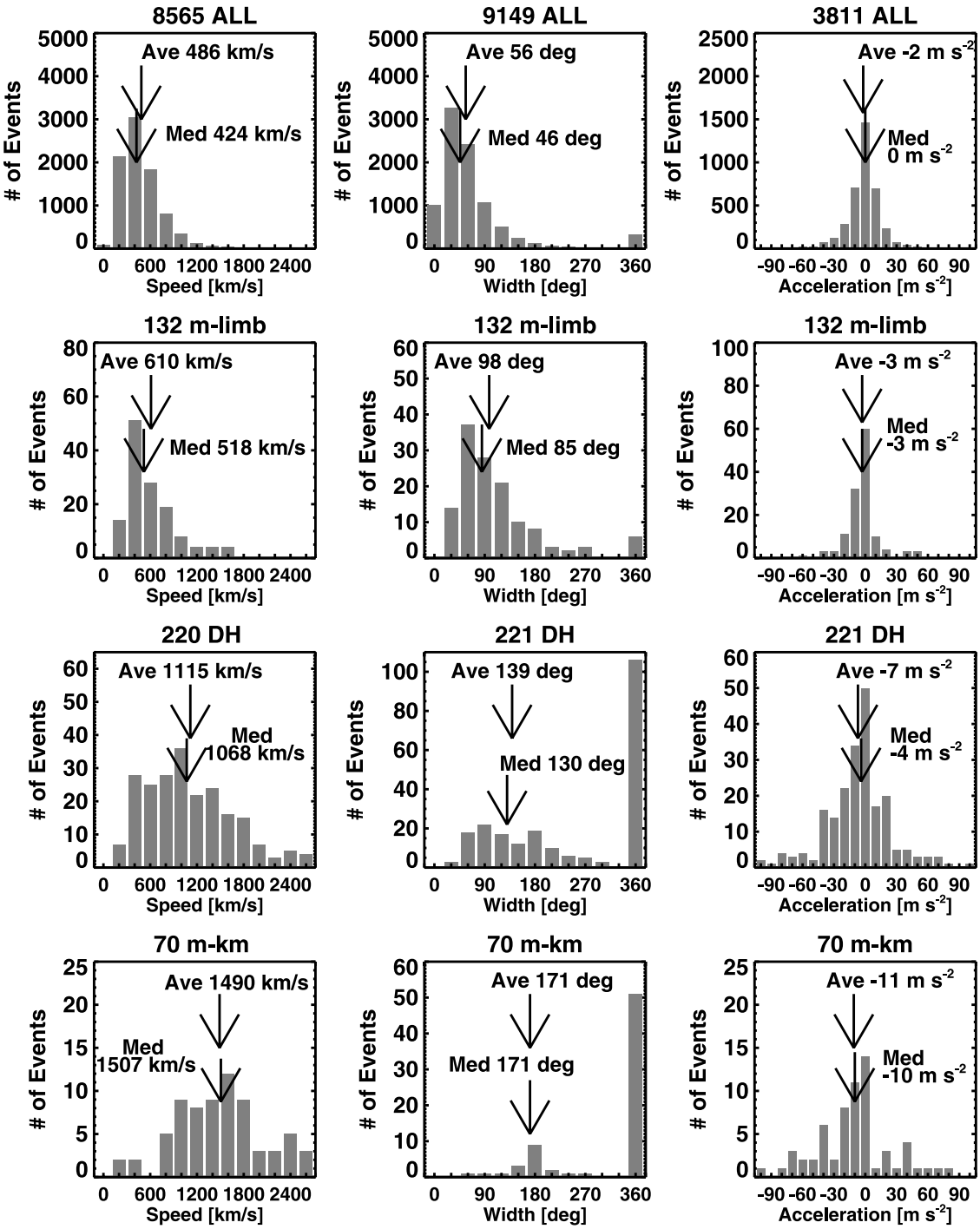

Figure 4. Properties of the general population (top row) CMEs compared with those of CMEs associated with metric (second row), DH (third row), and m-to-km (bottom row) type II bursts. We have shown the distributions of speed (first column), width (second column), and acceleration (third column) for the four populations of CMEs. All the parameters were measured in the sky plane and no attempt was made to correct for projection effects. The median and average values are shown on the plots for each distribution. The number of CMEs differs between columns because the speed and acceleration could not be measured for all CMEs. Note the progressive increases in average and median values in each column as one goes from the general population to populations of CMEs associated with metric, DH, and m-to-km type II bursts.

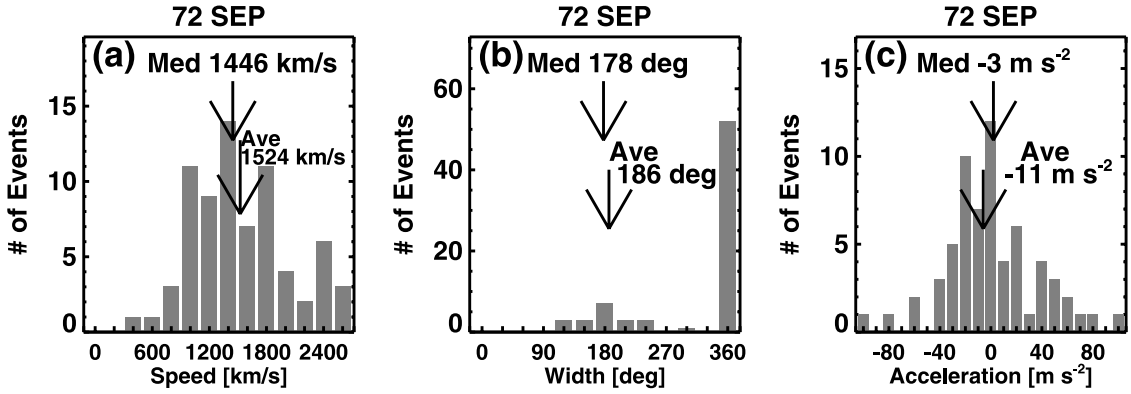

Figure 5. Distributions of speed, width, and acceleration of CMEs associated with large SEP events of cycle 23. Only events with simultaneous white light observations have been included. The average and median values of the distributions are shown on the plots. Note that the distributions are very similar to those of CMEs associated with m-to-km type II bursts (Figure 4, bottom row).

the type II emission between the metric and IP parts; the DH part started only at 4.5 MHz and ended at 500 kHz. The near-Sun environment of this event was also somewhat unusual. A large coronal hole was almost surrounding the active region from which the CME originated (see Figure 7). The coronal hole extended from the south polar region and extended to high northern latitudes. SOHO observations have demonstrated that the propagation of CMEs is severely affected by the presence of nearby coronal holes [*Gopalswamy et al.*, 2004, 2005a]. The reduced density (and hence higher Alfven speed) and enhanced flow in the coronal holes make the eastern flank of the shock rather weak, making it less efficient in accelerating particles. The presence of coronal holes between the Sun-observer line and the solar source of eruptions is known to reduce the intensity of SEPs [*Kunches and Zwickl*, 1999]. However, *Kahler* [2004] did not find any bias against SEP production in fast solar wind regions, although he used in situ composition signatures to identify fast streams rather than coronal holes.

[15] It must be pointed out that even though there happened to be the same number of large SEP events (71) and m-to-km type II bursts (72), the overlap is only 78%. Furthermore, not all SEP events associated with the m-to-km events are strictly large events (proton intensity in the >10 MeV channels >10 pfu). There were 11 events with intensity between 1 and 9 pfu, which are known as minor SEP events [*Gopalswamy et al.*, 2002], but they are much larger than the typical impulsive events [see e.g., *Reames*, 1999]. There are some large SEP events associated with type II bursts in the DH-to-km regimes without metric counterparts. These CMEs are also very energetic, but we did not include them in Table 1. In fact, there is a 100% association between large SEP events and DH type II bursts [*Gopalswamy*, 2003].

3.4. Type II Starting Frequencies

[16] The starting frequency of type II bursts is a good indicator of the approximate distance from the eruption center at which the shock forms and begins producing radio-emitting nonthermal electrons. The frequency of emission is related to the square root of the electron density in the vicinity of the shock. Thus high starting frequency implies that the shock is propagating through a high-density region and hence closer to the eruption region. We have compiled the starting frequencies of the metric component for the m-limb and m-to-km type II bursts from the SGD. In general, several observatories list a single type II event and usually the reports differ in staring times and frequency range. We have attempted to use the earliest time and the highest frequency reported for a given type II burst. Table 1 lists the starting frequency of the fundamental (F) component from the SGD. If a second harmonic component (H) has been identified by the reporting observatory, we have divided the reported starting frequency by 2 and listed in Table 1. Unfortunately, there is no F-H information for many type II bursts; the starting frequencies of these events are suffixed by a question mark in Table 1.

[17] Figure 8 shows the distribution of metric starting frequencies for the m-limb and m-to-km populations. Figures 8a and 8b include a subset of bursts whose starting frequencies definitely correspond to the F component. There were 80 m-limb and 46 m-to-km such events. For these events, the average starting frequencies are nearly the same for the two populations (101 MHz for m-limb and 111 MHz for m-to-km). This is opposite to what was found by *Robinson et al.* [1984] using a sample of only 16 metric type II bursts with IP counterparts. The distributions in Figures 8c and 8d were obtained assuming that all of the type IIs with unidentified F-H structures are F components. Finally, Figures 8e and 8f show plots obtained with the assumption that all the unidentified bursts are H components. In reality all the unidentified events will not fall into F or H groups but will be mixed. Nevertheless, the trend is clear that the m-limb events had slightly lower starting frequencies. *Robinson et al.* [1984] reported that ~78% of the metric type II bursts with IP counterparts had starting frequencies <45 MHz, compared to ~20% for all type II bursts. To make a similar comparison, we consider the number of events in the first bins of histograms in Figures 8a and 8b. We see that 27/80 (or 33%) of the m-limb events had starting frequency less than 50 MHz, while only 8/46 (or 17%) of the m-to-km events had such low starting

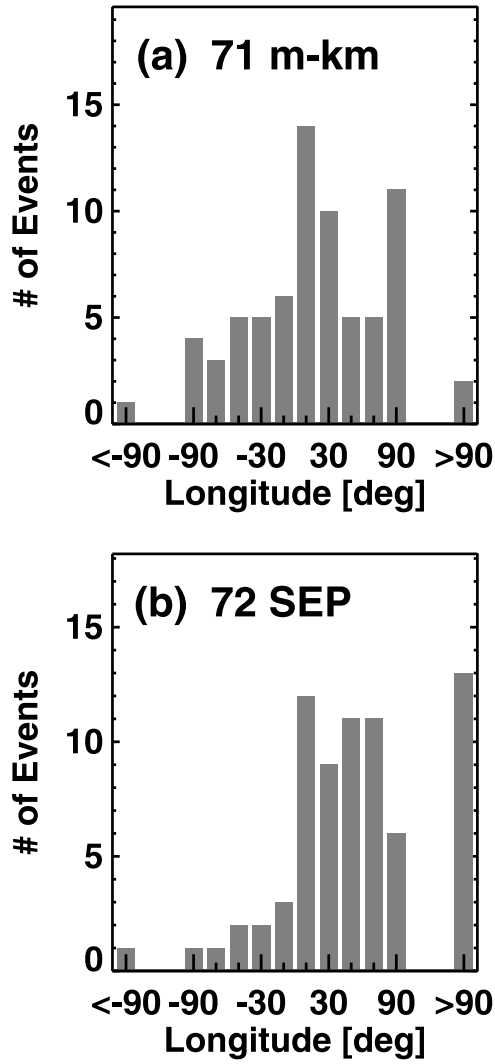

Figure 6. Comparison between the longitudes of solar sources of CMEs associated with m-to-km type II bursts and large SEP events. CMEs associated with large SEPs originate mainly in the western hemisphere, while CMEs associated with m-to-km type II bursts do not depend on solar longitude. This is one of the reasons for the lack of perfect association between SEP events and m-to-km type II bursts.

frequencies. Clearly, the results on starting frequencies obtained by *Robinson et al.* [1984] do not seem to hold.

3.5. CME Height at Metric Type II Onset

[18] Traditionally, the starting height of a type II burst is obtained assuming a radial density model in the corona because the emission frequency gives the local plasma density. Since we have CME measurements, we can directly obtain the type II height with the following assumptions: (1) The type II burst is formed at the location of the bowshock surrounding the CME, and (2) the shock standoff distance is very small so we can take the height of the CME leading edge to be the same as the maximum height of the shock. The actual height of the type II burst is likely to be smaller than the height of the CME leading edge if the type II burst is formed at the flanks of the shock where the condition for electron acceleration is known to be favorable [*Holman and Pesses*, 1983]. Figure 9 compares the distributions of CME leading edges at the onset times of metric type II bursts obtained by extrapolating the CME height-time measurements to the times of metric type II onsets. Extrapolations using both linear (left) and quadratic (right) fits to the height-time measurements have been used. Figures 9a and 9b show the CME leading edge heights for all the m-to-km type II bursts, for which the CME height extrapolated to the time of the corresponding metric type II burst is positive. Some heights were $<1\ R_S$ or <0 because the sources were close to the disk center, so the extrapolated heights are not actual heights. The average height at which the metric type II bursts start is $\sim 1.8\ R_S$ ($1.6\ R_S$) when we used linear (quadratic) fit. To avoid projection effects, we also considered a subset of m-to-km events for which the solar source is in the limb region (longitude 60° and above) and obtained the average height as 2.3 and 2.2 R_S for linear and quadratic fits (see Figures 9c and 9d), respectively. These heights are nearly identical to the corresponding heights for the m-limb population (2.2 R_S for linear fit and 2.1 R_S for quadratic fit). The similarity between CME leading edge heights of the m-to-km and m-limb population is also consistent with the similarity between the starting frequencies of the two populations. In other words, type II bursts form roughly at the same heights irrespective of whether or not an IP type II burst follows. *Robinson et al.* [1984] had suggested that the shocks responsible for the metric type II bursts form in the height range of $1.6-2\ R_S$, which is not too different from the heights of CME leading edges. However, the heights are the same for the m-limb and m-to-km type II bursts, which is different from *Robinson et al.* [1984] result that metric type II bursts followed by IP type II bursts have a lower starting frequency, implying a larger coronal height where the shock forms.

4. Discussion

[19] We studied the properties of CMEs associated with three populations of type II bursts: (1) those confined to the metric domain with no counterparts in the DH or km domains, (2) those observed in the DH domain, irrespective of the presence of counterparts in the metric and km domains, and (3) those having counterparts in all wavelength domains (metric, DH, and km). The CME kinetic energy has been found to organize the three populations: CMEs associated with population 1 are the least energetic, while those associated with population 3 are the most energetic. CMEs associated with population 2 are of intermediate energy. CMEs associated with type II bursts are more energetic than average CMEs. This result is consistent with that of *Lara et al.* [2003], who considered only populations 1 and 2, and thus is more complete. One might wonder about the population of type II bursts confined to the km domain with no counterparts in the m and DH domains. CMEs associated with these "purely km" type II bursts need not be more energetic than population 3 but have a different acceleration profile. These CMEs accelerate gradually and attain shock-driving capability only far into the IP medium when the speed becomes high enough to be super-Alfvenic. Statistical

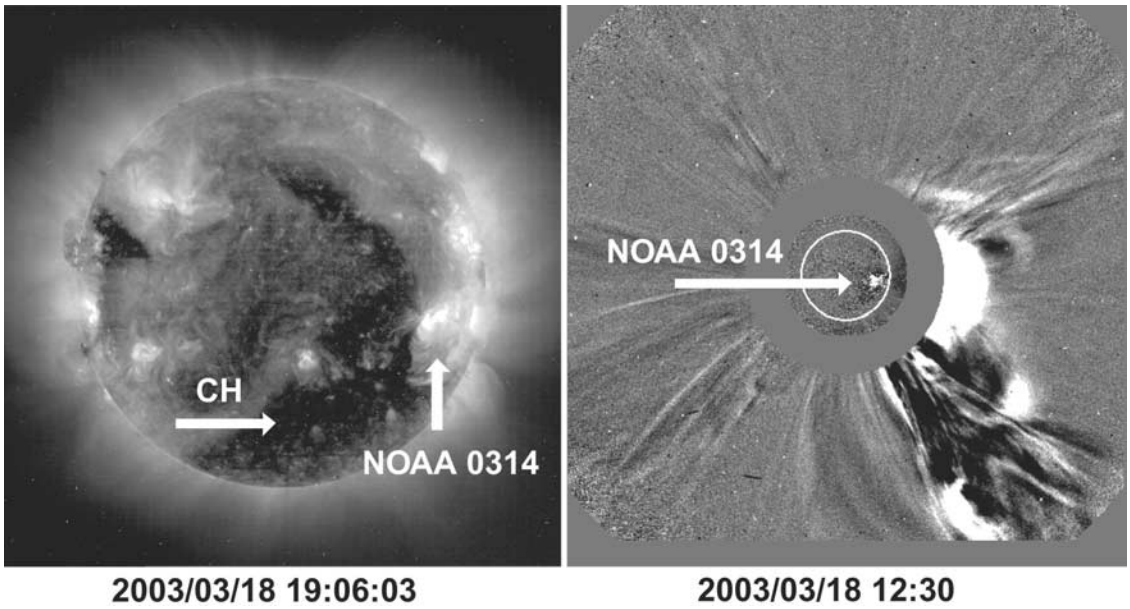

Figure 7. (left) A large coronal hole (CH, pointed by arrow) situated between the Sun-Earth line and the region of eruption (NOAA 0314). The image was obtained by SOHO/EIT in the 284 A band at 1906:03 UT on 18 March 2003. (right) SOHO/LASCO difference image at 1230 UT on the same day showing the CME above the west limb. The EUV manifestation of the eruption (dimming and flare brightening) as seen in the EIT 195 A difference is indicated by an arrow. See color version of this figure in the HTML.

properties of the purely km type II bursts will be reported elsewhere.

[20] The average speed, width, and acceleration were used as proxy to the kinetic energy that distinguishes the populations of CMEs associated with m, DH, and m-to-km type II bursts. The acceleration is not completely independent because the fastest CMEs tend to have the greatest deceleration due to the drag force in the corona and IP medium. This was shown to be the case for CMEs associated with DH type II bursts [*Gopalswamy et al.*, 2001b]. Thus the acceleration provides a consistency check. Ideally, one should obtain the kinetic energy using the measured mass and speed, but we have used the speed and width as proxy to the kinetic energy, since one can obtain CME mass estimates only for a subset of CMEs [*Vourlidas et al.*, 2002; *Gopalswamy*, 2004b]. Figure 10 shows that the CME mass is clearly correlated with the apparent width (correlation coefficient = 0.63). The plot includes all CMEs (for the period 1996–2003) with width $\leq$120°, irrespective of their source location. The regression line gives a mass of 2×10^{15} g for a width of 120°. This is higher than the mass of an average CME (6.9×10^{14} g) [see *Gopalswamy et al.*, 2005b] by a factor of 3. We also computed the mass of the 26 limb CMEs in Table 1 because the mass estimate is accurate for limb CMEs. The average mass of the 26 CMEs associated with the limb m-to-km CMEs in Table 1 was $\sim 9.8 \times 10^{15}$ g, more than an order of magnitude higher than the mass of the average CME. From the computed mass and speed, we computed the average kinetic energy of the limb CMEs in Table 1 as 1.8×10^{32} erg, which is more than two orders of magnitude larger than the kinetic energy of an average CME (5.2×10^{29} erg) [see *Gopalswamy et al.*, 2005b].

[21] The continuity from DH to km domains almost always holds because we can combine RAD1 and RAD2 spectral domains to track the bursts. However, this cannot be shown for the metric and longer wavelength type II bursts, although the continuity is certainly observed for some events [*Gopalswamy*, 2000; *Cliver et al.*, 2004]. Figure 3 is an example showing the continuity. Sometimes the metric and DH counterparts start simultaneously. One such event was reported by *Reiner* [2000], which had metric and DH counterparts present simultaneously at 60 MHz and 5 MHz. From a coronal density model, Reiner estimated that the metric type II burst corresponded to a disturbance moving at a speed of only 400 km/s, while the CME was moving at a speed of about 1050 km/s. The apparent height difference between metric and DH type II bursts was $\sim 2\ R_S$ when the two emissions were observed simultaneously. *Reiner* [2000] suggested that the metric and DH type II bursts were caused by two different shocks: the metric burst due to the blast wave from the associated flare and the DH and km type II bursts due to he CME-driven shock. Such discordant speeds were also found in a number of other events [*Reiner et al.*, 2001]. The lower speed of the disturbance responsible for the metric type II burst and the higher CME (responsible for the DH-km type II burst) are still consistent with a single shock scenario if the metric type II is caused by the shock flank (expected to be moving slower at lower coronal heights), while the longer wavelength burst is caused by the nose of the same shock (at a larger height moving faster). It is difficult to choose between the two possibilities without imaging observations simultaneously at metric and DH wavelengths. One has to go to space to image type II bursts at DH wavelengths, which may become possible

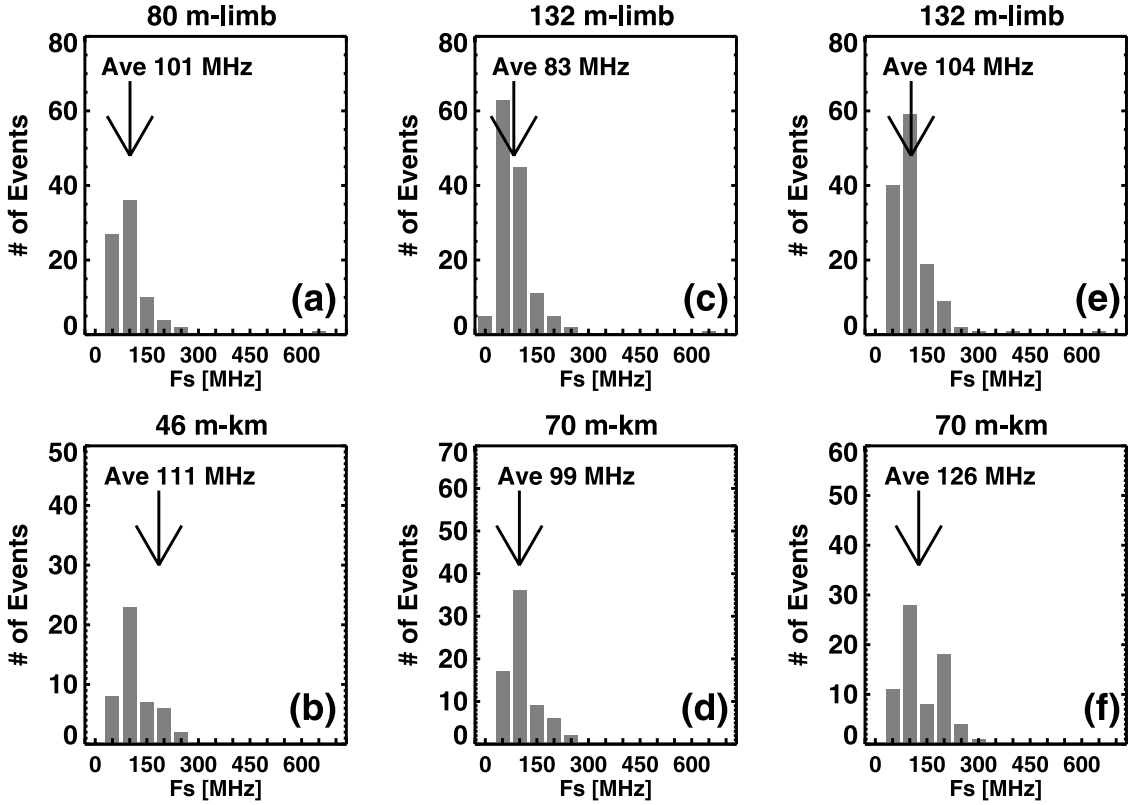

Figure 8. Distribution of starting frequencies (Fs) of metric component in the m-limb (top row) and m-to-km (bottom row) type II bursts. The two distributions look very similar. (a) and (b) Only those (80 m-limb and 46 m-to-km) bursts for which the mode of emission (fundamental, F, or second harmonic, H) has been identified. (c) and (d) All metric type II bursts assuming that the bursts with unidentified mode are in the F mode. (e) and (f) Similar to Figures 8c and 8d except that the bursts with unidentified mode are assumed to be in the H mode. The averages of all the distributions are marked on the plots. The average metric starting frequencies of the m-limb and m-to-km events are very close to each other.

by future missions such as the Solar Imaging Radio Array (SIRA) [*MacDowall et al.*, 2005].

[22] The starting frequencies and heliocentric distances of the metric type II bursts are virtually the same, independent of the existence of the longer wavelength counterparts. This may be due to the fact that the Alfven speed in the low corona is typically small, so CMEs with slightly above average energies can become super-Alfvenic to produce m type II bursts [see, e.g., *Gopalswamy et al.*, 2001a]: once the CME speed exceeds the local Alfvenic speed, a metric type II burst is produced, irrespective of how high the CME speed becomes. However, the kinetic energy of the CME is important in producing type II bursts at long wavelengths because the shock needs to be present and potent far into the IP medium. Thus we suggest that the result of *Robinson et al.* [1984] that the metric type II bursts with IP bursts have lower starting frequency may be an artifact due to a small sample size (16 events). They also did not have spectral coverage between 2 and 20 MHz, which makes the association between metric and IP type II bursts difficult. *Robinson et al.* [1984] also concluded that the shocks formed at a distance of 1.6–2.0 R_S. In the present study, we find that the CME leading edge is typically around 2.0 R_S at the time of type II onset. Since the shocks are likely to accelerate electrons at their flanks where quasi-perpendicularity might prevail, the agreement is reasonable.

[23] Although we do not see the starting frequency to be low, we do confirm *Robinson et al.* [1984] result that the flares associated with type II bursts with IP counterparts are stronger. Table 2 shows the distribution of X, M, and C-class flares for the m-limb and m-to-km type II bursts. B-class and smaller flares are listed as "others." The m-limb events were predominantly associated with C-and M-class flares (84%), while M-and X-class flares constitute the majority (86%) in the m-to-km events. Clearly, the m-to-km type II bursts are associated with bigger flares compared to the m-limb type II bursts. Association of the m-to-km events with the most energetic CMEs and largest flares reminds us of the "Big-flare Syndrome" [*Kahler*, 1982].

[24] Since the m-to-km type II bursts represent the most energetic disturbances, observing them provides a means of identifying the small fraction of CMEs that significantly disturb a large volume of the inner heliosphere. As can be seen in Figure 4, SOHO has observed more than 9000 CMEs during cycle 23 up to end of 2004. Over the same period, there were only 71 m-to-km type II bursts, which is only 0.8% of all the CMEs. Observing the m-to-km type II bursts provides an early warning of impending shock-

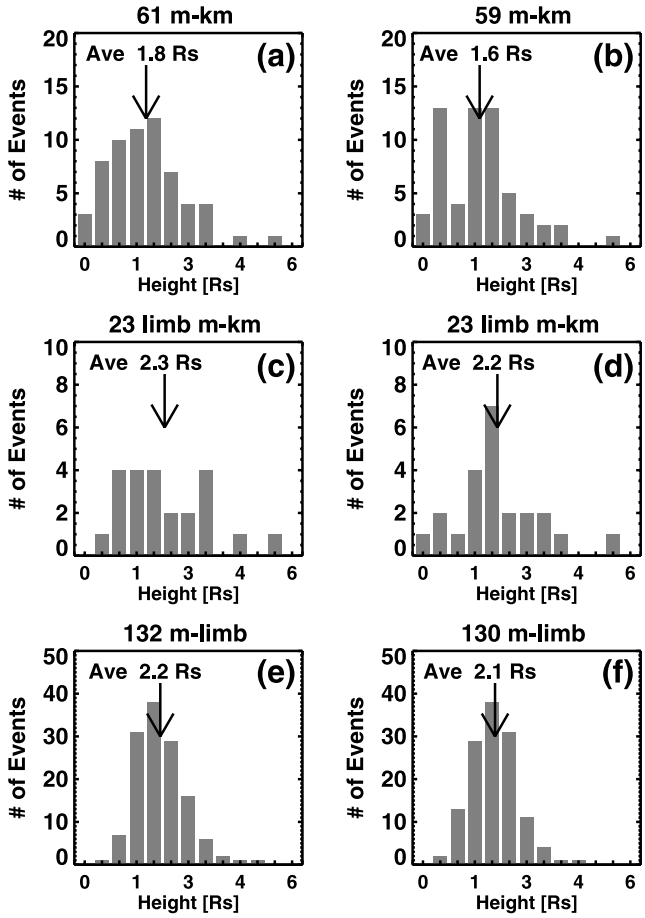

Figure 9. Distribution of the heights of CME leading edges at the onset times of metric type II bursts, obtained by (left) linear and (right) quadratic fits to the height-time measurements. (a) and (b) All the m-to-km type II bursts, for which the extrapolated CME height to the time of the corresponding metric type II burst is positive. Some heights were <1 R_S or <0 because the sources were close to the disk center, so the extrapolated heights are not actual heights. (c) and (d) Only those m-to-km type II bursts that had solar sources closer to the limb (longitudes 60° and above). (e) and (f) The m-limb type II bursts. Comparison between Figures 9c and 9e and Figures 9d and 9f shows that the CME leading edges are roughly at the same heights for metric type II bursts irrespective of whether or not an IP type II burst would follow.

related events (SEP events, energetic storms particle (ESP) events, storm sudden commencement, and IP CMEs) in the inner heliosphere. Although the lead time may be only tens of minutes for the >10 MeV SEPs, it may is more than half a day for the ESP events, sudden commencements, and ICME arrivals [*Gopalswamy et al.*, 2005b] and hence will prove to be useful for taking protective measures in space operations. The importance of a type II burst increases as it progresses to longer wavelengths. It takes ~1 hour for a typical type II burst to move from metric to km domains, so the lead time is still half a day or more for the shock arrival at 1 AU and all the related effects. The high degree of association (78%) between the m-to-km type II bursts and SEP events suggests that the underlying shocks are likely to produce ESP events.

5. Conclusions

[25] Exploiting the uniform and extended high quality-data on radio bursts (Wind/WAVES) and CMEs (SOHO/LASCO) we have studied the properties of CMEs associated with a special population of type II radio bursts, characterized by emission components in all of the spectral domains (metric, DH, and km). We compared their properties with those of the general population of CMEs and of CMEs associated with type II bursts in the metric and DH domains. We found that the CME kinetic energy organizes these bursts. CMEs with very low energy do not produce type II bursts; type II bursts confined to the metric domain are associated with CMEs of moderate energy, slightly higher than that of the general population. More energetic CMEs produce the DH Type II bursts, which occur at several solar radii from the Sun. CMEs of the highest energy produce type II bursts that have counterparts in all of the spectral domains (m-to-km). The m-to-km type II bursts imply that the CME-driven shock is present and strong enough to produce radio emission over a large range of distances from the Sun. This finding has a direct

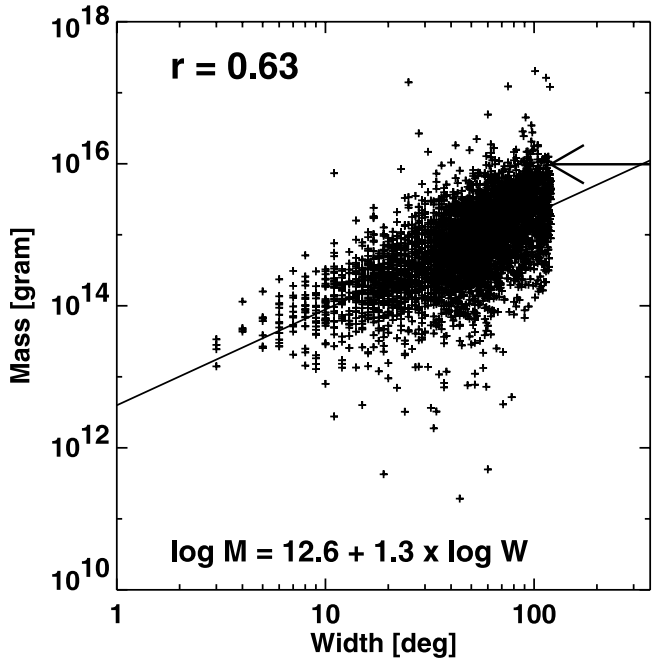

Figure 10. Scatter plot between the mass (M) and apparent width (W) for 4138 CMEs in the period 1996–2003 (inclusive), for which mass measurement was possible. The correlation coefficient (r = 0.63) is marked. Note that the true width of halo CMEs cannot be known due to the occulting disk, so we omitted them in the correlation. From other considerations, we know that halo CMEs represent an energetic population because they are significantly faster and wider than the general population. The regression line and its equation are shown on the plot. The arrow mark points to the average mass of the 26 CMEs associated with the m-to-km limb events in Table 1.

Table 2. Flare Sizes of the m-Limb and m-to-km Type II Bursts

	X	M	C	Other	Total
m-to-km	30 (42%)	31 (44%)	6 (8%)	4(6%)	71 (100%)
m-Limb	4 (3%)	53 (40%)	58 (44%)	17 (13%)	132 (100%)

implication to the study of the heliospheric disturbances: CMEs that drive shocks in the m-to-km wavelength domains are likely to propagate to large distances into the heliosphere to form the merged interaction regions. The CME energy is also commensurate with the flare sizes: the m-to-km population was mostly associated with M and X-class flares, while the bursts confined to the metric domain were predominantly associated with C and M-class flares. We also compared the metric starting frequencies of the m-to-km type II bursts with those of type II bursts confined to the metric domain. We did not find a significant difference between the two. In fact, the m-to-km bursts had a slightly higher starting frequency, opposite to what was found by *Robinson et al.* [1984]. We also did not find a large fraction of low starting frequency metric type II bursts in the m-to-km population. The CME height at the metric onset time of the radio bursts also did not show any difference between the two populations. The Alfven speed profile in the corona seems to be responsible for this result. Finally, we also found a high degree of association between m-to-km type II bursts and SEP events. The small number of m-to-km bursts not associated with SEP events had their solar sources poorly connected to the observer near Earth. While the SEP events detected at Earth preferentially occur in the western solar hemisphere, the m-to-km type II bursts have no such requirement due to the wide beaming of the radio emission. This means that m-to-km events originating from the eastern hemisphere and from behind the east limb may be important for other locations in the inner heliosphere. Thus the m-to-km type II bursts are also indicative of CMEs, shocks, and the associated SEPs propagating toward other destinations in the solar system such as Mars that are of interest to human exploration. Less than 1% of the 9000 CMEs observed during 1996–2004 were associated with the m-to-km type II bursts. Therefore the m-to-km bursts can isolate the small fraction of CMEs that are likely to have significant impact on the inner heliosphere from a space weather point of view.

[26] **Acknowledgments.** The authors thank A. Vourlidas for providing mass measurements for the limb events in Table 1. Part of this effort was supported by NASA/LWS and NSF/SHINE (ATM 0204588) programs. The WAVES instrument on board Wind was designed and built as a joint effort of the Paris-Meudon Observatory, the University of Minnesota, and the Goddard Space Flight Center. SOHO is a project of international cooperation between ESA and NASA.

[27] Shadia Rifai Habbal thanks Dale E. Gary and another referee for their assistance in evaluating this paper.

References

Boischot, A., A. C. Riddle, J. B. Pearce, and J. W. Warwick (1980), Shock waves and type II radio bursts in the interplanetary medium, *Solar Phys.*, *5*, 397.

Bougeret, J.-L., et al. (1995), Waves: The Radio and Plasma Wave Investigation on the Wind spacecraft, *Space Sci. Rev.*, *71*, 231.

Brueckner, G. E., et al. (1984), The large angle spectroscopic coronagraph (LASCO), *Solar Phys.*, *162*, 357.

Cane, H. V., and R. G. Stone (1984), Type II solar radio bursts, interplanetary shocks, and energetic particle events, *Astrophys. J.*, *282*, 339.

Cliver, E. W., D. F. Webb, and R. A. Howard (1999), On the origin of solar metric type II bursts, *Solar Phys.*, *187*, 89.

Cliver, E. W., S. W. Kahler, and D. V. Reames (2004), Coronal shocks and solar energetic proton events, *Astrophys. J.*, *605*, 902.

Delaboudiniere, J.-P., et al. (1995), EIT: Extreme-ultraviolet imaging telescope for the SOHO Mission, *Solar Phys.*, *162*, 291.

Gopalswamy, N. (2000), Type II solar radio bursts, in *Radio Astronomy at Long Wavelengths*, *Geophys. Monogr. Ser.*, vol. 119, edited by R. G. Stone et al., p. 123, AGU, Washington, D.C.

Gopalswamy, N. (2003), Solar and geospace connections of energetic particle events, *Geophys. Res. Lett.*, *30*(12), 8013, doi:10.1029/2003GL017277.

Gopalswamy, N. (2004a), Recent advances in the long-wavelength radio physics of the Sun, *Planet. Space Sci.*, *52*, 1399.

Gopalswamy, N. (2004b), Interplanetary radio bursts, in *Solar and Space Weather Radiophysics*, edited by D. E. Gary and C. O. Keller, p. 305, chap. 15, Springer, New York.

Gopalswamy, N., M. L. Kaiser, R. P. Lepping, S. W. Kahler, K. Ogilvie, D. Berdichevsky, T. Kondo, T. Isobe, and M. Akioka (1998), Origin of coronal and interplanetary shocks: A new look with Wind spacecraft data, *J. Geophys. Res.*, *103*, 307.

Gopalswamy, N., M. L. Kaiser, B. J. Thompson, L. Burlaga, A. Szabo, A. Lara, A. Vourlidas, S. Yashiro, and J.-L. Bougeret (2000), Radio-rich solar eruptive events, *Geophys. Res. Lett.*, *27*, 1427.

Gopalswamy, N., A. Lara, M. L. Kaiser, and J.-L. Bougeret (2001a), Near-sun and near-Earth manifestations of solar eruptions, *J. Geophys. Res.*, *106*, 25,261.

Gopalswamy, N., S. Yashiro, M. L. Kaiser, R. A. Howard, and J. Bougeret (2001b), Characteristics of coronal mass ejections associated with long-wavelength type II radio bursts, *J. Geophys. Res.*, *106*, 29,219.

Gopalswamy, N., S. Yashiro, G. Michaek, M. L. Kaiser, R. A. Howard, D. V. Reames, R. Leske, and T. von Rosenvinge (2002), Interacting coronal mass ejections and solar energetic particles, *Astrophys. J.*, *572*, L103.

Gopalswamy, N., S. Yashiro, A. Lara, M. L. Kaiser, B. J. Thompson, and P. Gallagher (2003), Large solar energetic particle events of cycle 23: A global view, *Geophys. Res. Lett.*, *30*(12), 8015, doi:10.1029/2002GL016435.

Gopalswamy, N., S. Yashiro, S. Krucker, G. Stenborg, and R. A. Howard (2004), Intensity variation of large solar energetic particle events associated with coronal mass ejections, *J. Geophys. Res.*, *109*, A12105, doi:10.1029/2004JA010602.

Gopalswamy, N., S. Yashiro, G. Michalek, H. Xie, R. P. Lepping, and R. A. Howard (2005a), Solar source of the largest geomagnetic storm of cycle 23, *Geophys. Res. Lett.*, *32*, L12S09, doi:10.1029/2004GL021639.

Gopalswamy, N., S. Yashiro, Y. Liu, G. Michalek, A. Vourlidas, M. L. Kaiser, and R. A. Howard (2005b), Coronal mass ejections and other extreme characteristics of the 2003 October-November solar eruptions, *J. Geophys. Res.*, *110*, A09S15, doi:10.1029/2004JA010958.

Hoang, S., and P. Zlobec (1997), Characteristics of solar kilometer-wave type II radio bursts, *Hvar Obs. Bull.*, *21*(1), 57.

Holman, G. D., and M. E. Pesses (1983), Solar type II radio emission and the shock drift acceleration of electrons, *Astrophys. J.*, *267*, 837.

Howard, R. A., D. J. Michels, N. R. Sheeley, and M. J. Koomen (1982), The observations of a coronal transient directed at Earth, *Astrophys. J.*, *263*, L101.

Kahler, S. W. (1982), The role of the big flare syndrome in correlations of solar energetic proton fluxes and associated microwave burst parameters, *J. Geophys. Res.*, *87*, 3439.

Kahler, S. W. (2004), Solar fast-wind regions as sources of shock energetic particle production, *Astrophys. J.*, *603*, 330.

Kaiser, M. L., M. J. Reiner, N. Gopalswamy, R. A. Howard, O. C. St. Cyr, B. J. Thompson, and J.-L. Bougeret (1998), Type II radio emissions in the frequency range from 1–14 MHz associated with the April 7, 1997 solar event, *Geophys. Res. Lett.*, *25*, 2501.

Kunches, J., and R. Zwickl (1999), The effects of coronal hole on the propagation of solar energetic protons, *Radiat. Meas.*, *30*, 281.

Lara, A., N. Gopalswamy, S. Nunes, G. Muñoz, and S. Yashiro (2003), A statistical study of CMEs associated with metric type II bursts, *Geophys. Res. Lett.*, *30*(12), 8016, doi:10.1029/2002GL016481.

MacDowall, R. J., et al. (2005), The Solar Imaging Radio Array: space based imaging of solar, heliopheric, magnetospheric, and atrophysical sources at frequencies below the ionospheric cutoff, in *From Clark Lake to the Long Wavelength Array*, *PASP Conf. Proc.*, edited by N. E. Kassim et al., Astron. Soc. of the Pacific, San Francisco, Calif., in press.

Malitson, H. H., J. Fainberg, and R. G. Stone (1973), Observation of a type II solar radio burst to 37 Ro, *Astrophys. Lett.*, *14*, 111.

Payne-Scott, R., D. E. Yabsley, and J. G. Bolton (1947), Relative times of arrival of solar noise on different radio frequencies, *Nature*, *160*, 256.

Pinter, S., V. P. Grigorieva, K. Kecskemety, and K. Kudela (1984), Observation of solar radio bursts of type II and III at kilometer wavelengths

from PROGNOZ-8 during STIP interval XII (10 April–21 June 1981), in *Solar/Interplanetary Intervals, Proceedings of the STIP Symposium Held 4–6 August 1982*, edited by M. A. Shea, D. F. Smart, and S. M. P. McKenna-Lawlor, p. 119, Book Crafters, Huntsville, Ala.

Reames, D. V. (1999), Particle acceleration at the Sun and in the heliosphere, *Space Sci. Rev.*, *90*, 413.

Reiner, M. J. (2000), Interplanetary type II radio emissions associated with CMEs, in *Radio Astronomy at Long Wavelengths*, *Geophys. Monogr. Ser.*, vol. 119, edited by R. G. Stone et al., p. 137, AGU, Washington, D. C.

Reiner, M. J., M. L. Kaiser, J. Fainberg, and R. G. Stone (1998), A new method for studying remote type II radio emissions from coronal mass ejection-driven shocks, *J. Geophys. Res.*, *103*, 29,651.

Reiner, M. J., M. L. Kaiser, N. Gopalswamy, H. Aurass, G. Mann, A. Vourlidas, and M. Maksimovich (2001), Statistical analysis of coronal shock dynamics implied by radio and white-light observations, *J. Geophys. Res.*, *106*, 29,989.

Robinson, R. D., R. T. Stewart, and H. V. Cane (1984), Properties of metre-wavelength solar bursts associated with interplanetary type II emission, *Solar Phys.*, *91*, 159.

Vourlidas, A., D. Buzasi, R. A. Howard, and E. Esfandiari (2002), paper title, in *Solar Variability: From Core to Outer Frontiers*, *ESA SP-506*, vol. 1, edited by A. Wilson, p. 91, Eur. Space Agency, Paris.

Wild, J. P., and L. L. McCready (1950), Observations of the spectrum of high-intensity solar radiation at metre wavelengths. I. The apparatus and spectral types of solar burst observed, *Austral. J. Sci. Res.*, *A3*, 387.

Yashiro, S., N. Gopalswamy, G. Michalek, O. C. St.Cyr, S. P. Plunkett, N. B. Rich, and R. A. Howard (2004), A catalog of white light coronal mass ejections observed by the SOHO spacecraft, *J. Geophys. Res.*, *109*, A07105, doi:10.1029/2003JA010282.

E. Aguilar-Rodriguez, N. Gopalswamy, M. L. Kaiser, S. Nunes, and S. Yashiro, NASA Goddard Space Flight Center, Code 695.0, Building 21, Room 260, Greenbelt, MD 20771, USA. (gopals@fugee.gsfc.nasa.gov)

R. A. Howard, Naval Research Laboratory, Code 7660, Washington, DC 20375, USA.